Understanding Reaction Mechanisms of Nicotinamide Adenine Dinucleotide (NADH) with Lithium Cobalt Oxide and Other Metal Oxide Nanomaterials

SCHOLARONE™
Manuscripts

1
2
3
4
5
6
7
8
9
10
11
12
13
14
15
16
17
18
19
20
21
22
23
24
25
26
27
28
29
30
31
32
33
34
35
36
37
38
39
40
41
42
43
44
45
46
47
48
49
50
51
52
53
54
55
56
57
58
59
60

While many studies have probed the behavior of nanomaterials in the environment, few studies have attempted to address the detailed chemical pathways controlling how nanomaterials interact with biomolecules and organisms. We recently showed that high-valent Co-containing nanomaterials can oxidize NADH (an essential biomolecule) and in turn NADH reduces $LiCoO_2$ and thereby accelerates release of Co^{2+} from the nanoparticle. This oxidation-reduction interaction creates two parallel pathways to environmental impact. The present work systematically studies the specific sub-molecular components of NADH and how each component is involved in the nanoparticle-biomolecule interaction. Our data show that phosphate groups play a key role in the interaction of NADH with $LiCoO_2$ nanosheets by binding strongly to the $LiCoO_2$ surface and thereby facilitating electron transfer from the nicotinamide group to $LiCoO_2$. Similar results are also presented for ribose functionalities and using Mn_2O_3 as a second example high-valent oxide. These results are important to environmental science because they provide key insights into cross-species unifying mechanisms of interaction between nanomaterials and biological systems of potential environmental relevance. The direct interaction of nanoparticles with biomolecules that are part of cellular respiration has important consequences for understanding and predicting the potential environmental consequences of nanomaterials.

1
2
3
4
5
6
7
8
9
10
11
12
13
14
15
16
17
18
19
20
21
22
23
24
25
26
27
28
29
30
31
32
33
34
35
36
37
38
39
40
41
42
43
44
45
46
47
48
49
50
51
52
53
54
55
56
57
58
59
60

ARTICLE

Understanding Reaction Mechanisms of Nicotinamide Adenine Dinucleotide (NADH) with Lithium Cobalt Oxide and Other Metal Oxide Nanomaterials

Catherine E. Kruszynski Earl[a], Austin H. Henke[a], Elizabeth D. Laudadio[a], and Robert J. Hamers[a*]

Abstract

High-valent metal oxides such as $LiCoO_2$ and related materials are of increasing environmental concern due to the large-scale use in lithium-ion batteries and potential for metal ion release into aqueous systems. A key aspect of the environmental chemistry of these materials is the potential role redox chemistry plays in their transformations as well as their influence on the surrounding environment (i.e., biomolecules, organisms etc.). In recent work, we showed that $LiCoO_2$ (a common lithium-ion battery cathode material) oxidizes nicotinamide adenine dinucleotide (NADH), an essential molecule for electron transport, and enhances Co release from $LiCoO_2$. In the present work, we investigated the mechanism of interaction by examining the role of the ribose, phosphate, adenosine, and the nicotinamide components of NADH in the transformation of $LiCoO_2$ nanoparticles. To build an understanding of the interaction mechanism, we used fluorescence spectroscopy to measure the changes in redox state and inductively coupled plasma-mass spectrometry (ICP-MS) to measure the changes in dissolved Co. Our results reveal the importance of surface binding, via the phosphate functionality, in initiating the redox transformation of both the $LiCoO_2$ and the NADH. Observations from X-ray photoelectron spectroscopy (XPS) data show that molecules containing phosphate were bound to the surface of the nanoparticles and those without that functionality were not. We further established the generality of the results with $LiCoO_2$ by examining other high-valent transition metal oxides. This surface binding effect has implications for understanding how other phosphorylated species can be transformed directly in the presence of high-valent metal oxide nanomaterials.

[a.] Dept. of Chemistry, University of Wisconsin-Madison, 1101 University Avenue, Madison WI 53706, USA

Introduction

Assessing the environmental impact of nanomaterials requires an understanding of both how nanoparticles transform the environment and how the nanoparticles are transformed by the environment.[1-4] Among the nanomaterials being produced on commercial scales, metal oxides are the most commonly used composition, and the release of metals from metal oxides represents a possible route to toxicity for many organisms in the environment.[5-9] Consequently, there is great interest in understanding the factors that influence transformation of metal oxides as well as the chemical mechanisms by which metal oxides interact with biological systems. Among these, $LiCoO_2$ and the broader family of "NMC" compositions ($LiNi_xMn_yCo_{1-x-y}O_2$, x,y < 1) represents a family of related compositions whose use is expanding rapidly due to their role as the cathode materials in lithium ion batteries. Due to this high volume of production[10-13] (>50 kg per electric vehicle) and known toxicity of Co to different organisms,[6, 14] $LiCoO_2$ and related NMC compositions can serve as an effective model system for understanding environmental transformations and impact of high-volume nanomaterials used in emerging energy storage technologies.[15-19]

Transformation of metal oxides and release of free metals typically requires a protonation step to form metal hydroxides at the nanoparticle surface. In the case of high-valence metal oxides, however, the oxidation state of the metal is also of critical importance because metal ions in high oxidation states frequently have much lower solubility compared with metal ions in lower oxidation state.[20, 21] For example, $Co(OH)_3$ has a solubility product of ~ 10^{-43}, while that of $Co(OH)_2$ is 2.5×10^{-16}.[20, 22] These values indicate that at pH=7, Co^{3+} can only be present up to concentration of ~10^{-21} M and is therefore effectively insoluble, while Co^{2+} can be stable at concentrations close to 1 M. Since Co exists in the +3 state within solid $LiCoO_2$, it would be expected to exhibit high stability in aqueous media. However, studies of $LiCoO_2$ and related molecules under laboratory conditions have frequently observed significant release of Co at concentrations vastly exceeding the aforementioned values.[15, 23, 24] As a result, it can be concluded the oxidation-reduction chemistry must also be taking place, with the metal oxide being reduced by one or more solution components. We recently showed that NADH, an important molecule in cellular respiration, interacts strongly with $LiCoO_2$ via oxidation-reduction ("redox") chemistry. NADH reduces the Co^{3+} to Co^{2+} and accelerates the release of Co^{2+} into the aqueous phase, while NADH itself becomes oxidized. These two processes: (1) accelerated release of Co and (2) oxidation of NADH to NAD^+, both have the potential to lead to biological

impact. While the influence of NADH is strong, work to date has not elucidated the salient molecular features of NADH responsible for inducing these transformations, nor has prior work established whether the above mechanisms can be generalized to a broader range of compositions and environmentally relevant molecules.

Here, we aim to understand the specific features of NADH that are necessary in order to activate this process. The NADH molecule (Figure 1) is made up of four primary components: 1) a nicotinamide group that is the major center of redox in cellular processes, 2) an adenine nucleotide, 3) ribose sugars, and 4) a bridging diphosphate. To understand how each of these functionalities interacts with $LiCoO_2$, we investigated the interaction of the nanoparticles with NADH and with several commercially available compounds bearing the salient components. Figure 1 shows the molecules investigated here: D-ribose-5-phosphate ("Ribose-PO_4"),1-methyl-1,4-dihydronicotinamide ("Nico"), and adenosine monophosphate (AMP). We hypothesized that if phosphate was responsible for surface attachment, Ribose-PO_4 and AMP would exhibit greater binding to $LiCoO_2$. Alternatively, if the nicotinamide group is responsible for redox reaction without phosphate binding required, Nico would reproduce the enhanced Co release and a decrease in fluorescence as seen with NADH. If both binding and reducing strength are needed in the same molecule to see any effect, these experiments could show that both components of NADH are needed to react with $LiCoO_2$. Furthermore, we tested particles exposed to both Nico and Ribose-PO_4 to see if there were synergistic effects of separate molecules to recapture what was seen with NADH. Lastly, we studied the dissolution behavior of $LiCoO_2$ in the presence of other ribose derivatives (Figure 1) to understand the importance of the phosphate moiety.

Since ribose sugars are also redox active, in their ring-opened form, the amount of Co released after exposure can be used to determine the effect of the phosphate moiety. We hypothesized that molecules with the phosphate moiety would show an increase in Co release similar to what we observe with NADH, even though NADH does not show a similar ring-opened form, because they are both redox active. We extended this investigation to nanomaterials of metal oxides other than $LiCoO_2$, such as NiO and Mn_2O_3, since transition metals sometimes behave similarly in environmental transformations, such as coordination with small organic acids,[25-28] reduction by bacteria,[29-35] or effects of pH.[36] However, this may not be the case on the nanomaterial scale, with $LiCoO_2$ being a Li-intercalation compound, or since the reaction with NADH is potentially surface-driven (i.e., site-specific). Determining if reaction mechanisms of $LiCoO_2$ with reducing biomolecules can be extended to other metal oxide compounds would be useful in assessing environmental toxicity of nanomaterials and understanding natural interaction of microbes with mineral surfaces.

Experimental
Nanoparticle synthesis and characterization.

Sheet-like nanoparticles of cobalt hydroxide $Co(OH)_2$ and $LiCoO_2$ were synthesized following procedures we described previously.[37] Briefly, $Co(OH)_2$ nanosheets were prepared by precipitation, and the $Co(OH)_2$ precursor was then converted to $LiCoO_2$ using a molten salt flux consisting of a 6:4 molar ratio of $LiNO_3:LiOH$ at 200 °C. All solutions in this study were prepared from nanopure water (Barnstead Genpure System, resistivity ≥ 18.2 MΩ·cm). Mn_2O_3 (~50 nm diameter) and NiO (~80 nm diameter) nanoparticles were obtained from U.S. Research Nanomaterials. While the supplier labelled these materials as MnO_2 and Ni_2O_3, respectively, we performed x-ray diffraction analysis to check the crystal structure and phase purity; our measurements (Supporting Information, Figure S1) showed that the actual compositions correspond to Mn_2O_3 and NiO, respectively. Here, we refer to the nanoparticles based on their actual composition.

Powder x-ray diffraction (XRD) patterns were obtained for each sample using a Bruker D8 Advance diffractometer equipped with a copper Kα source and 6 mm slit width. Samples for XRD analysis were prepared by affixing nanoparticle powder onto a B-doped silicon crystal zero-diffraction plate (MTI Corporation) by drop-casting a slurry. Specific surface area measurements of ~0.1 g vacuum-dried samples were determined by nitrogen physisorption (Micromeritics Gemini VII 2390 surface area analyzer) and Brunauer-Emmett-Teller (BET) analysis. [38] The nanoparticles were imaged using scanning electron microscopy (SEM) (LEO Supra55 VP field-emission), with typical images shown in Supporting Information Fig. S2. These images show that $LiCoO_2$ nanoparticles form in a sheet-like morphology, with typical thickness of ~5 nm and diameter ~30 nm, consistent with previous characterization data.[39, 40] $Co(OH)_2$ also form at sheet-like plates (See Fig. S2B). [39] All samples were prepared by drop-casting a dilute solution of nanoparticles onto a P-doped silicon wafer. Dynamic light scattering (DLS) (Malvern Zetasizer Nano ZS) was used to measure hydrodynamic diameter of the nanoparticles. Samples were prepared by sonicating a 200 mgL^{-1} nanoparticle/ultrapure water solution at 6 kHz for one hour and then diluting the solutions to 10 mgL^{-1} immediately before analysis.

Media composition.

To facilitate understanding of how redox properties of nanoparticles impact biological systems, we use a model bacterial growth medium with minimal constituents ("minimal medium" with dextrose), prepared using nanopure water with various salts, 4-(2-hydroxyethyl)-1-piperazineethanesulfonic acid (HEPES) buffer, and dextrose, adjust to pH=7 with NaOH; the full composition is described in the Supporting Information (Table S1). This composition was chosen based on its widespread use in biological studies and as a model medium to link the transformations investigated here with their biological impact, to be investigated separately.

NADH reduced disodium salt (Sigma Aldrich), 1-methyl-1,4-dihydronicotinamide (Cayman Chemical), D-ribosephosphate disodium salt (Sigma Aldrich), D(-)-ribose (Sigma Aldrich), and Methyl beta-D-Ribofuranoside (TCI America) were obtained from commercial sources and used as received. Solutions were

prepared for each molecule of interest by dissolving in minimal medium to a concentration of 0.5 mM. This concentration was chosen because it is relevant to concentrations of these molecules found in cells [41, 42] and it produces suitable fluorescence signals for NADH and Nico solutions. In the case of solutions with two species combined, solutions had a concentration of 0.5 mM of each molecule. Nanoparticles were introduced at 1 mg·mL^{-1} concentration into 4 mL vials. The sealed vials were protected from light and placed on an orbital shaker for 24 h. The samples were then centrifuged at 13,100 × g for 20 min (Eppendorf MiniSpin plus) and the supernatant was collected and filtered through 0.1 μm porosity syringe filter cartridges (Millex VV) to remove residual nanoparticles, a separation procedure that we have used in previous studies and confirmed removal of nanoparticles.[43] All experiments were performed in at least triplicate, and error bars represent standard error of the mean.

Molecules Investigated.

In the work reported here, we investigated several molecules of interest. Figure 1 shows the structure of these molecules. Within NADH, the nicotinamide moiety at the upper right is the functionality generally associated with the oxidation-reduction of NADH.[44, 45] In addition, NADH also contains an adenosine monophosphate and a ribose sugar ring. In Fig. 1, Ribose and Ribose-PO$_4$ are able to tautomerize into the linear form depicted in Fig. 1C and 1E; this linear "aldose" structure presents an aldehyde group that is generally associated with the ability of ribose to act as a reducing sugar. Notable, however, the ribose within NADH is not able to undergo this tautomerization due to the presence of other substituent groups at the relevant position around the sugar ring.
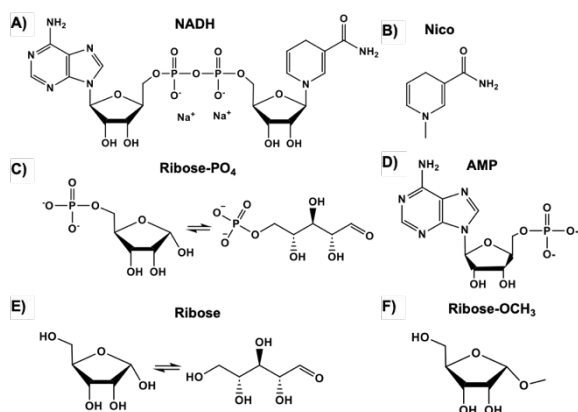

Figure 1. Molecular structures of A) NADH, B) 1-methyl-1,4-dihydronicotinamide (Nico), C) ribose 5-phosphate (Ribose-PO$_4$), D) adenosine monophosphate (AMP), E) Ribose, and F) methyl beta-D-ribofuranoside (Ribose-OCH$_3$)

Quantification of NADH and Nico via fluorescence.

The concentration of NADH in samples was determined via fluorescence using an ISS K2 photon-counting spectrofluorometer, using measurement conditions similar to those reported previously.[46, 47] Samples were placed in a fused silica cuvette at room temperature, excited at λ_{ex} = 338 nm, and the emission spectrum was measured between λ_{em} = 400 and λ_{em} = 550 nm with a step size $\Delta\lambda$ = 1 nm and integration time of 1 s per step. NADH exhibits an emission peak at $\lambda_{em} \approx 455$ nm, whereas oxidized NAD$^+$ does not. The intensity was background-subtracted using a blank consisting of minimal medium with dextrose. To ensure consistency of fluorescence measurements across the entire time scan of this study, on a daily basis we also measured the fluorescence intensity from a solid tetraphenylbutadiene standard and normalized spectra to this standard. Concentrations of NADH were determined using a calibration curve made using NADH standards prepared at different concentrations in media. Solutions of Nico were treated in the same manner, except with different excitation and emission wavelengths optimized experimentally. Nico contains the same fluorescent nicotinamide moiety as NADH, but to our knowledge its fluorescence properties have not been reported previously. We measured the spectroscopic properties of 0.5 mM Nico in an excitation-emission matrix range of λ_{ex} = $300-400$ nm and λ_{em} = $340-540$ nm, yielding the results shown in Supporting Information Figure S3. Based on these measurements, we used λ_{ex} = 328 nm for excitation and λ_{em} = $340-540$ nm (with peaks at 382 nm and 450 nm) for further quantification studies. To confirm that the fluorescence of Nico arises only from its intact (reduced) form, we performed an oxidative control experiment (Figure S4); this control experiment shows that only the reduced form of Nico shows significant fluorescence.

Quantification of metal release.

We used inductively coupled plasma mass spectrometry (ICP-MS) to measure dissolved metal ion concentrations in samples after centrifugation/filtration. Preliminary measurements were performed on Shimadzu ICPMS-2030, but later samples were analyzed using an Agilent 8900 ICP-QQQ triple-quadrupole IC-MS. Samples were diluted 500:1 dilution to reduce salt concentrations from the minimal media with dextrose matrix and were acidified using 2.5% HNO$_3$ before analysis. We quantified metal concentrations using ^{59}Co, ^{60}Ni, and ^{55}Mn ion signals and referencing to a 100 ppb yttrium internal standard. Each sample was measured in triplicate by ICP-MS and the average intensities were used for quantification. Concentrations were determined using calibration curves made using serial dilution from 1 g·L^{-1} certified reference materials. Standards were diluted and acidified in the same manner as the unknowns.

Measuring surface binding of molecules using X-ray Photoelectron Spectroscopy (XPS).

To determine whether the different NADH components interact with the surface of $LiCoO_2$, nanoparticles were collected post-exposure and washed with ultrapure water to release any molecules not strongly adsorbed to the surface of the particles. Measurements were taken on a Thermo K-alpha XPS using an Al Kα source (1486.6 eV photon energy) at a 45° take-off angle. Survey spectra were taken at a pass energy of 200 eV and resolution of 1 eV/step. For P(2p) and N(1s) high-resolution spectra we used a 50 eV pass energy and 0.200 eV/step resolution. XPS data were analyzed using CasaXPS, using a Shirley background correction [48, 49] and a GL(30) mixed Gaussian-Lorentzian line shape for peak-fitting analysis.[50] All energies were calibrated to the 284.8 eV binding energy of adventitious carbon.[51] Samples were prepared by drop-casting a slurry of nanomaterials in water onto a silicon wafer and dried overnight. Each molecule was measured in triplicate. Areas from the high-resolution XPS peaks for each element were used to calculate atomic percentages at the surface as reported previously.[43]

Results and discussion

Impacts of NADH, Nico, and Ribose-PO₄ on Co release from LiCoO₂.

While NADH can be sub-divided in different ways, we first investigated the impact of the nicotinamide group (Fib. 1B), the ribose-PO_4, (Fig. 1C) and the AMP group(Fig. 1D). We evaluated the impact of these molecules on the solubilization of Co from $LiCoO_2$ by measuring the concentration of Co released into solution after $LiCoO_2$ nanoparticles were added into solutions of these molecules, using procedures described in the Experimental section. Fig. 2A shows the resulting Co concentrations. In Fig. 2A, the data show that NADH increases Co release from $LiCoO_2$ compared with the concentration of Co released in media alone, consistent with our prior work.[43] Additional experiments show that this increase is proportional to the concentration of NADH. Surprisingly, introducing Nico, which also contains the nicotinamide group, induces almost no Co release beyond that observed in the media alone. Ribose-PO_4 increases release from $LiCoO_2$, despite the absence of the nicotinamide group; however, as noted above, Ribose-PO_4 can
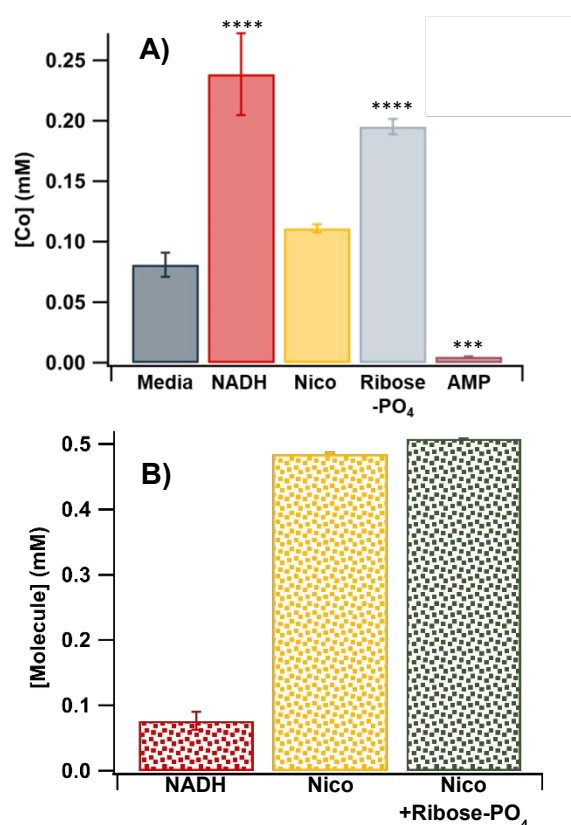

Figure 2. A) Dissolved Co concentrations determined by ICP-MS for $LiCoO_2$ after 24h, 1 mg·mL^{-1} exposure to media containing the indicated molecules. Each exposure compared to the Co release from media alone with one-way ANOVA with Dunnett's multiple comparisons test. *** for p< 0.001 and **** for p< 0.0001 B) Post-exposure biomolecule concentrations from NADH, Nico, and from a mixture of 0.5 mM Nico +0.5 mM Ribose-PO_4 as measured by fluorescence spectroscopy.

tautomerize to form a free aldehyde. Finally, AMP hinders release of Co to values lower than those observed in the media alone. The data in Fig. 2A show that the presence of the nicotinamide moiety alone is not sufficient to account for the rapid Co release induced by NADH, and that the ability of NADH to accelerate the release of Co is more complex than just the role of NADH as a reducing agent.

Determining changes in Nico oxidation state after LCO exposure.

As a complement to the Co release studies, we performed studies to determine to what extent exposure to $LiCoO_2$ alters the oxidation state of the nicotinamide group within NADH and within Nico. Optimal wavelengths were determined experimentally and described in the Experimental section. The nicotinamide group is fluorescent only in the reduced form; therefore, measurements of the fluorescence intensity probe the amount of NADH and/or Nico that remains in the starting (reduced) form. We also conducted control experiments to verify that oxidation of NADH and of Nico quenches their fluorescence, as described in Supporting Information (Fig. S4). Fig. 2B shows the remaining reduced molecule concentrations as determined by their fluorescence after solutions of 0.5 mM NADH and of 0.5 mM Nico were exposed to 1 mg·mL^{-1} dispersions of $LiCoO_2$ nanoparticles. These data show that $LiCoO_2$ effectively oxidized NADH but does not oxidize Nico. As a further control experiment, we exposed $LiCoO_2$ NPs to a solution containing both Nico and Ribose-PO$_4$, both at 0.5 mM, to test whether for any possible synergistic or interfering influence; these results showed that the presence of Ribose-PO$_4$ did not influence the interactions of Nico.

The ability of $LiCoO_2$ to oxidize the nicotinamide group when incorporated into the NADH molecule but not when incorporated into the Nico molecule is surprising. The formal reduction of NAD$^+$ to NADH is generally considered in two steps: NAD$^+$ + e- →NAD• with E'$_{NAD+/NAD•}$ = -920 mV and followed by NAD• + H$^+$ + e- →NADH with E'$_{NAD•/NADH}$ = +282 mV, where the potentials are formal potentials at pH=7. Together these yield the two-electron formal potential of E'$_{NAD+/NADH}$ =-320 mV. [52] While the reduction potential associated with Nico has not been reported previously, data for similar nicotinamide derivatives show that substitution at the N position has only a very weak

inductive effect that shifts the reduction potential to even slightly more negative values.[44] Thus, we conclude that the reduction potential of Nico should be more than sufficient to reduce Co^{3+} in $LiCoO_2$ to Co^{2+}, with corresponding oxidation of Nico. Yet, we observe that Nico alone has little effect.

Phosphate as an active participant in the redox between $LiCoO_2$ and NADH.

A second important difference between NADH and Nico is the presence of the phosphate groups in NADH, which are absent in Nico. Previous studies have shown that free phosphate groups from phosphoric acid and related species bind strongly to $LiCoO_2$ surfaces.[37, 40] To understand the possible role of the phosphate groups in NADH and related molecules, we compared the Co release from $LiCoO_2$ nanoparticles after exposure to each of the three molecules (1) ribose, (2) Ribose-OCH$_3$, and (3) Ribose-PO$_4$. As shown in Figure 1, of these three molecules, only the native ribose and Ribose-PO$_4$ have a hydroxyl group at the 1-position that is required to tautomerize into the aldehyde group characteristic of reducing sugars. Ribose-OCH$_3$ is therefore not a reducing sugar. Fig. 3 shows the Co release data for these three molecules and two additional control molecules. Among the group of ribose, Ribose-OCH$_3$ and Ribose-PO$_4$, only ribose-PO$_4$ induces the release of Co into

Figure 4. Atomic coverages of N (Fig. 4A) and P (Fig. 4B) on $LiCoO_2$ nanoparticles after 24 hr exposure to listed molecules calculated from high resolution XPS measurements. Spectra taken after particles had been washed with water releasing any loosely bound species. Dark-colored bars indicate data for molecules containing the element of being probed; light colors show data for molecules not containing the element being probed. Both N-containing and P-containing molecules are present in the starting aqueous media that is present for all studies. Each exposure compared to the atomic coverage from media alone with one-way ANOVA with Dunnett's multiple comparisons test. * for p<0.05, *** for p< 0.001, and **** for p< 0.0001
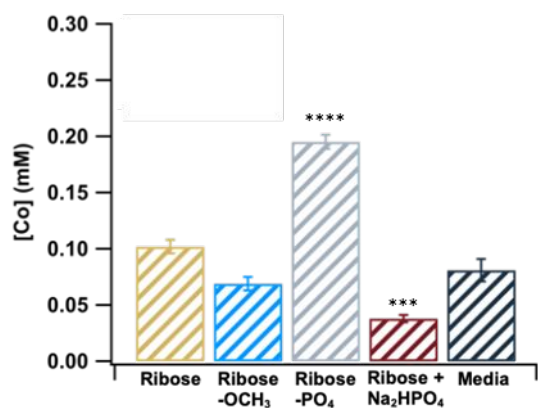
Figure 3. Co release from $LiCoO_2$ nanoparticles measured using ICP-MS after exposure to ribose derivatives listed above. Media and Ribose-PO$_4$ data taken from Figure 2 to show comparison. Each exposure compared to the Co release from media alone with one-way ANOVA with Dunnett's multiple comparisons test. *** for p< 0.001 and **** for p< 0.0001
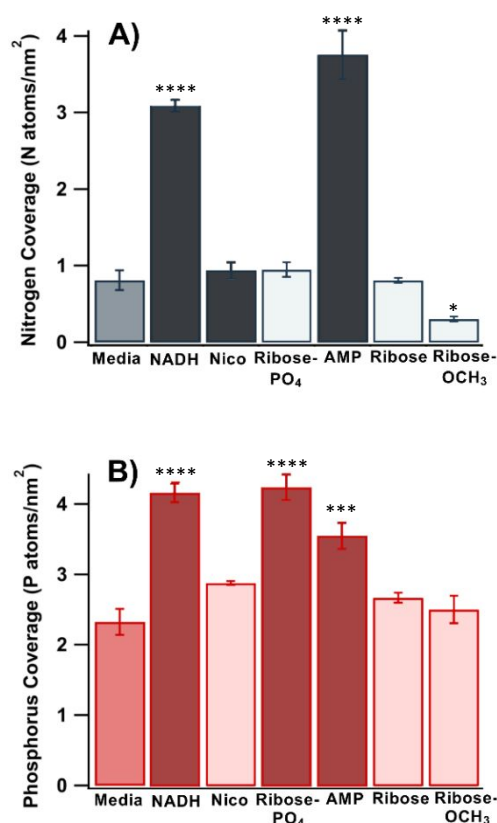
solution to an extent comparable to that of NADH. This result shows that the phosphate group plays an important role in accelerating the metal release. As a further confirmatory test, we exposed LiCoO$_2$ nanoparticles to media ribose solution with added NaH$_2$PO$_4$ at the same concentration (0.5 mM), adjusted to pH=7. At this pH the phosphate groups are expected to be present as H$_2$PO$_4^-$ and HPO$_4^{2-}$ in nearly equal concentrations. As shown in Fig. 3, the presence of these free phosphate species reduces the amount of Co released to values even lower than those observed in the media alone, even with ribose present. These data show that free phosphate groups inhibit interaction of ribose with LiCoO$_2$, while phosphate chemically linking to ribose has an activating role. Together, these observations suggest that binding of phosphate groups to the surface is a key factor controlling molecular interactions with the LiCoO$_2$ surface.

To evaluate the possible importance of direct surface binding, we used x-ray photoelectron spectroscopy (XPS) to characterize the extent of surface binding using the N(1s) and P(2p) emission intensities. By using emission of Co (from LiCoO$_2$) as an internal standard and using well known atomic sensitivity factors and inelastic mean free paths, the XPS data can be translated into approximate atomic coverages, as described in the Supporting Information. Figure 4A and 4B show the N and P coverage, respectively, after LiCoO$_2$ nanoparticles were exposed to NADH, Nico, and AMP, along with a control sample exposed to the media alone. Due to the presence of sodium phosphate, HEPES buffer, and ammonium chloride in the minimal media, the spectra show some N and P present for all molecules. However, in Fig. 4A, it is apparent that NADH and AMP (both of which contain N as part of their molecular structures) bind to the LiCoO$_2$ surface while Nico does not increase the N coverage beyond that produced by the media alone. Nico, Ribo-PO$_4$, and Ribose do not impact the amount of

N on the surface, while Ribo-OCH$_3$ may even reduce the N coverage compared to the media alone. Fig. 4B shows XPS data for phosphorus. Again, some P is observed from the phosphate species present in the starting medium, but NADH, Ribose-PO$_4$, and AMP further increase the amount of surface phosphorus. Ribose-OCH$_3$, Ribose, and Nico do not impact the surface coverage of phosphorus.

The N(1s) XPS data (Fig. 4A) show that only among those molecules with N as part of their structure, only NADH and AMP show increased surface binding compared to the control (media) sample, while Nico does not. The P(2p) data (Fig. 4B) show that all three molecules with phosphate groups (NADH, Ribose-PO$_4$, and AMP) show significantly increased binding compared to the media control, while others do not. Among the molecules investigated, NADH and Ribose-PO$_4$ are the only two that significantly increase the release of Co from LiCoO$_2$. Taken together, our data indicate that the ability of NADH and of Ribose-phosphate to induce release of Co is due to combination of the phosphate group and the redox-active group (nicotinamide for NADH, and a reducible ribose group for Ribose-PO$_4$) *chemically linked together in close proximity on the same molecule*.

As depicted in Figure 5A, our results suggest that NADH binds to the LiCoO$_2$ surface via its phosphodiester group (as shown in Fig. 4) and then induces an electron-transfer into the LiCoO$_2$, reducing the Co into its soluble Co^{2+} form (Fig. 2A) and oxidizing the nicotinamide group (as evidence by loss of fluorescence in Fig. 2B). The ribose ring of NADH cannot tautomerize and presumably acts as an electron conduit between the nicotinamide group and the phosphate-surface complex. In the case of Ribose-PO$_4$, the ability to tautomerize into the linear aldose form allows it to act as a reducing agent, while binding of the adjacent phosphate group facilitates electron transfer to the LiCoO$_2$, solubilizing the Co much like in
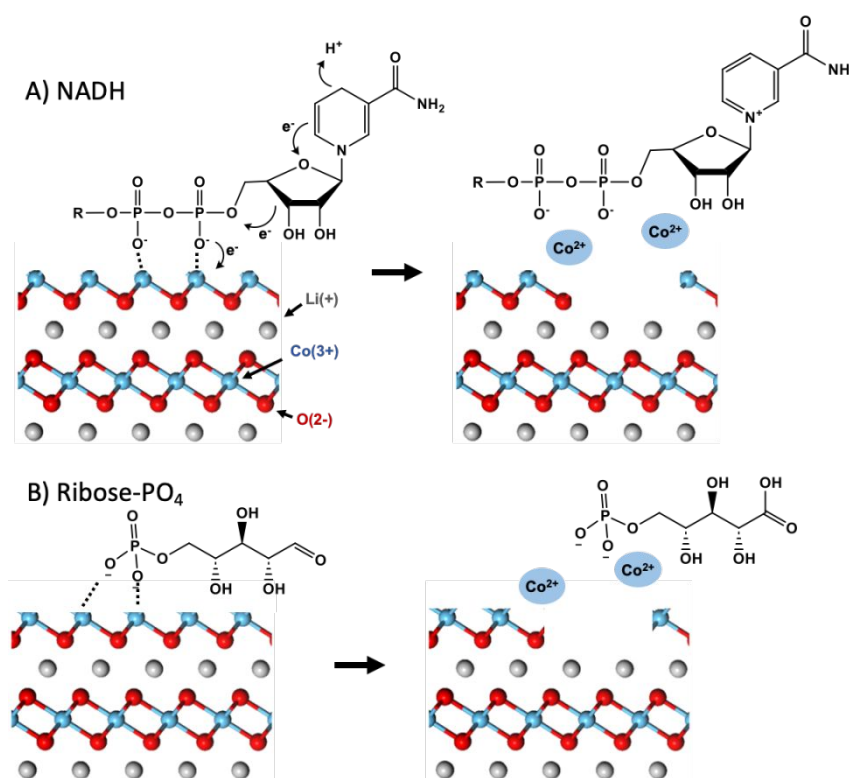

Figure 5. A) Proposed mechanism for the redox reaction of NADH with LiCoO$_2$. NADH binds to LiCoO$_2$ via its phosphate groups, after which Co^{3+} is reduced by the transfer of electrons from nicotinamide to ribose, to Co^{3+}. The products are solubilized Co^{2+} and NAD$^+$. The reaction is not fully balanced to account for release of oxygen atoms from the lattice, which are likely to react with H$^+$ to form H$_2$O. B) Proposed mechanism for ribose phosphate interacting with LiCoO$_2$.

the case of NADH. We note that the oxidized form of NADH has been well studied and gives a final product like that depicted in Fig. 5A, the oxidation of Ribose-PO_4 depicted in Fig. 5B is not known with certainty. However, since Co release can only occur via reduction of Co from Co^{3+} (In $LiCoO_2$) to Co^{2+}(aq), the concentrations of Co observed in Fig. 3 establish that Ribose-PO_4 must be oxidized upon interaction with $LiCoO_2$.

The strong binding of phosphate to $LiCoO_2$ can also act as a barrier to Co release; for example, exposure to AMP strongly decreases Co release (Fig. 2A) and in the combination of NaH_2PO_4 with Ribose (Fig. 3) decreases Co release compared with Ribose alone. These results indicate that in realistic media, the degree to which a given molecule impacts Co release depends both on the molecule's reducing ability and the possibility of competitive binding between different PO_4-containing species.
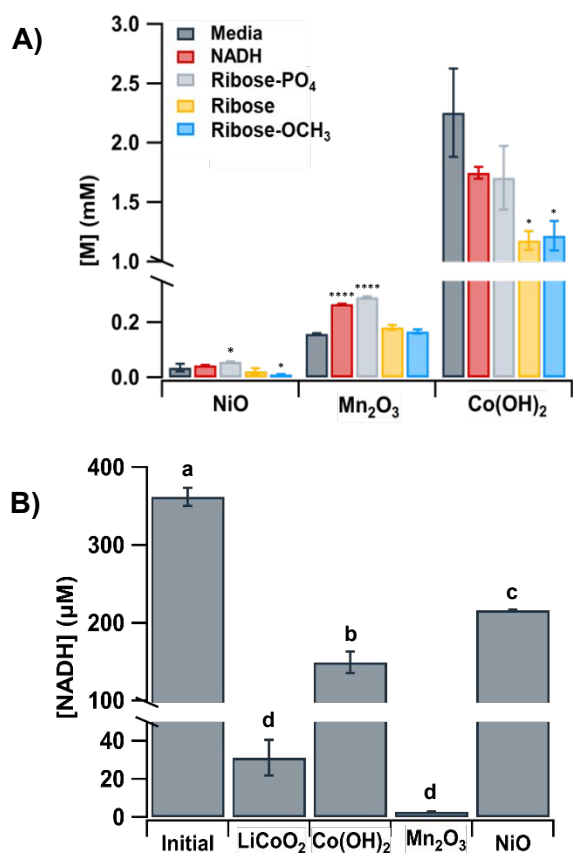

Figure 6. A) Metal ion release measured with ICP-MS from nanomaterials after 24-hr exposure. Each nanoparticle exposure compared to the metal release from the media alone using a one-way ANOVA with Dunnett's multiple comparisons test. n=3 * for p<0.05, **** for p<0.0001. B) NADH concentrations measured by fluorescence spectroscopy remaining after 24 hr exposure to each transition metal-containing nanomaterial. Letters indicate significant difference as determined by one-way ANOVA with Tukey HSD post hoc (n=3 p< 0.05).

Our results show that despite acting as a reducing agent, the ability of NADH to promote Co release from $LiCoO_2$ is highly

dependent on its ability to bind to the surface. One likely reason for this requirement is the inherently unfavorable nature of the initial (one-electron) oxidation of NADH to NAD•. As noted above at pH=7 the oxidation of NADH to NAD• is endoergic (unfavorable), while the second step to form NAD^+ is highly exoergic. One consequence of this scenario is that transfer of the *first* electron from NADH to $LiCoO_2$ has a barrier that must be overcome. We hypothesize that the reason binding to the $LiCoO_2$ surface enhances the reactivity is that surface binding provides a higher local concentration of NADH at the solid surface, and a long surface residence time then facilitates the endoergic first step in electron transfer. Similar considerations also likely hold for the enhancement of Co release induced by Ribose-PO_4 but not by free ribose or Ribose-OCH_3.

Generalization to other metal oxides

While the data in Fig. 1-5 are specific to $LiCoO_2$, some other high-valence metal oxides have low solubility but can be solubilized by reducing the metal cations. To test this idea more broadly, we conducted studies using several other metal oxides, including Mn_2O_3 as an example high-valence nanoparticle and using $Co(OH)_2$ and NiO as examples of low-valence compounds. To further characterize the metal oxide nanoparticles, we measured specific surface areas using BET nitrogen adsorption isotherms and also measured hydrodynamic diameters and zeta potentials in nanopure water, giving the results shown in Table 1. We note that $LiCoO_2$ and $Co(OH)_2$ nanoparticles have a thin sheet-like morphology. Because this non-spherical morphology disobeys the spherical approximation that is made in converting raw DLS data into size and zeta potential,[40] we refer to these as the *apparent* hydrodynamic diameter and *apparent* zeta potential and use the resulting values only as a guide. While there are some differences in specific surface area and hydrodynamic diameter between different nanoparticle compositions, the differences are comparatively small. Additionally, comparisons are made within each nanoparticle type to investigate whether the addition of biomolecules increases the metal cation release from the particles as opposed to comparing the release of metals from each nanoparticle.

Table 1. Nitrogen adsorption calculated surface area and hydrodynamic diameter of nanoparticles.

	Specific area, $m^2 \cdot g^{-1}$	Apparent hHydrodynamic diameter, nm	Apparent Zeta Potential
$LiCoO_2$	97.1 ± 0.2	170 ± 40	-16.7 ± 1.4
$Co(OH)_2$	80.36 ± 1.2	114.8 ± 6	21.0 ± 3.9
Mn_2O_3	24.42 ± 0.08	146.4 ± 10	-28.1 ± 0.9
NiO	18.55 ± 0.7	111.0 ± 15	-28. 8 ± 2.0

Figure 6A shows concentrations of solubilized metal ([M]) after these metal oxides are introduced into solutions of each of the indicated molecules. The high-valence oxide Mn_2O_3 shows increased metal concentration in solution in the presence of NADH and Ribose-PO_4, while Ribose, and Ribose-OCH_3 have little or no effect. This behavior is similar to that observed for $LiCoO_2$. In contrast, metal release from $Co(OH)_2$ is

mildly suppressed by each of the four investigated molecules, but in all cases Co release from $Co(OH)_2$ is much higher than that from $LiCoO_2$ due to the high intrinsic solubility of Co^{2+} compounds.

Measurements of the impact on NADH show more dramatic differences between metal oxides. Fig. 6B shows the residual fluorescence from NADH after exposure to the nanoparticles of interest. The high-valence oxides $LiCoO_2$ and Mn_2O_3 yield severe decreases in NADH fluorescence intensity, which we attribute to oxidation of NADH to the non-fluorescent NAD^+ form. In contrast, the +2 oxidation state compounds $Co(OH)_2$ and NiO yield only slight decreases in NADH concentration; these small decreases in NADH are likely due to (non-reactive) adsorption of NADH onto the surface of the particles. The results in Fig. 6A and 6B show that NADH induces metal release from both Mn_2O_3 and from $LiCoO_2$ by reducing the metals to lower oxidation states that are more highly soluble. Concurrently, the NADH is oxidized to NAD^+. In contrast, the data for $Co(OH)_2$ and NiO show that the metals are not being reduced to more soluble forms and NADH is not being oxidized by the materials.

Overall, these dissolution results for Mn_2O_3 and NiO are promising in that they confirm our hypothesis that NADH acts as a reducing agent to enhance ion release specifically for high oxidation state metal oxides, and that the mechanism can be applied to other metal oxides outside of $LiCoO_2$. In both cases, the presence of phosphate groups facilitates the electron-transfer process.

Conclusions

In our previous work we found that NADH interacted with $LiCoO_2$ via an electrochemically driven process in which NADH induced electron transfer to the $LiCoO_2$, thereby solubilizing the Co from the insoluble Co^{3+} to soluble Co^{2+} form at the surface of the nanoparticle and oxidizing the NADH.[43] Both of these processes – release of transition metals, and oxidation of molecules involved in cellular respiration – may be important in understanding the fundamental chemical mechanisms controlling the environmental impact of nanoparticles. Our present investigation sheds light on the important molecular and sub-molecular factors that control these molecule-nanoparticle reactivities. In particular, the present work shows that the ability of molecules to act as reducing agents is not necessarily sufficient to induce significant interaction with nanoparticles, but that the presence of phosphate groups of NADH and Ribose-PO_4 play a key role in facilitating electron transfer from these molecules to $LiCoO_2$ surfaces by binding the molecules to the surface of $LiCoO_2$. While demonstrated here for $LiCoO_2$ and Mn_2O_3, the phenomena described here may also be important for a wider range of nanoparticle compositions, particularly those that are insoluble in high oxidation states [20] such that electron-transfer to the nanoparticle enhances solubility.

Understanding the role of specific sub-molecular functional groups, such as phosphate, on nanoparticle interactions with biomolecules may be important in understanding the fundamental chemical interactions that drive biological responses to nanoparticle exposure at the cellular and organism level. Many other biomolecules and biopolymers, including some that play important roles in cellular electron transport, contain phosphate groups. Examples include flavin adenine dinucleotide (FAD) and related flavins[53, 54] DNA, and RNA. While DNA oxidation has been reported in response to nanoparticle exposure,[23, 24] the detailed molecular origins remain unknown. Studies like those reported here may provide key insights into the fundamental chemical origins of nanoparticle interactions with living systems in the environment.

Author Contributions

Catherine E. Kruszynski: Investigation; methodology; formal analysis; verification; writing-original draft; writing – review and editing; visualization.

Austin H. Henke: Investigation; methodology; formal analysis; verification; writing-original draft; writing – review and editing; visualization.

Elizabeth D. Laudadio: Methodology; investigation.

Robert J. Hamers: Conceptualization, Writing-Review and Editing; Project administration; formal analysis; visualization; funding acquisition.

Conflicts of interest

There are no conflicts to declare.

References

1. M. R. Wiesner, G. V. Lowry, P. Alvarez, D. Dionysiou and P. Biswas, Assessing the risks of manufactured nanomaterials, *Environ. Sci. Technol.*, 2006, **40**, 4336-4345.
2. S. J. Klaine, P. J. J. Alvarez, G. E. Batley, T. F. Fernandes, R. D. Handy, D. Y. Lyon, S. Mahendra, M. J. McLaughlin and J. R. Lead, Nanomaterials in the environment: Behavior, fate, bioavailability, and effects, *Environ. Toxicol. Chem.*, 2008, **27**, 1825-1851.
3. R. D. Handy, F. von der Kammer, J. R. Lead, M. Hassellov, R. Owen and M. Crane, The ecotoxicology and chemistry of

manufactured nanoparticles, *Ecotoxicology*, 2008, **17**, 287-314.

4. G. V. Lowry, K. B. Gregory, S. C. Apte and J. R. Lead, Transformations of Nanomaterials in the Environment, *Environ. Sci. Technol.*, 2012, **46**, 6893-6899.

5. A. A. Keller and A. Lazareva, Predicted Releases of Engineered Nanomaterials: From Global to Regional to Local, *Environ. Sci. Technol. Lett.*, 2014, **1**, 65-70.

6. D. J. Paustenbach, B. E. Tvermoes, K. M. Unice, B. L. Finley and B. D. Kerger, A Review of the Health Hazards Posed by Cobalt, *Crit Rev Toxicol*, 2013, **43**, 316-362.

7. A. Rastogi, M. Zivcak, O. Sytar, H. M. Kalaji, X. L. He, S. Mbarki and M. Brestic, Impact of Metal and Metal Oxide Nanoparticles on Plant: A Critical Review, *Front. Chem.*, 2017, **5**, 16.

8. M. F. Hochella, D. W. Mogk, J. Ranville, I. C. Allen, G. W. Luther, L. C. Marr, B. P. McGrail, M. Murayama, N. P. Qafoku, K. M. Rosso, N. Sahai, P. A. Schroeder, P. Vikesland, P. Westerhoff and Y. Yang, Natural, incidental, and engineered nanomaterials and their impacts on the Earth system, *Science*, 2019, **363**.

9. N. Zuverza-Mena, D. Martinez-Fernandez, W. C. Du, J. A. Hernandez-Viezcas, N. Bonilla-Bird, M. L. Lopez-Moreno, M. Komarek, J. R. Peralta-Videa and J. L. Gardea-Torresdey, Exposure of engineered nanomaterials to plants: Insights into the physiological and biochemical responses-A review, *Plant Physiol. Biochem.*, 2017, **110**, 236-264.

10. L. Li, J. B. Dunn, X. X. Zhang, L. Gaines, R. J. Chen, F. Wu and K. Amine, Recovery of metals from spent lithium-ion batteries with organic acids as leaching reagents and environmental assessment, *J. Power Sources*, 2013, **233**, 180-189.

11. W. G. Lv, Z. H. Wang, H. B. Cao, Y. Sun, Y. Zhang and Z. Sun, A Critical Review and Analysis on the Recycling of Spent Lithium-Ion Batteries, *ACS Sustain. Chem. Eng.*, 2018, **6**, 1504-1521.

12. M. A. Hannan, M. M. Hoque, A. Mohamed and A. Ayob, Review of energy storage systems for electric vehicle applications: Issues and challenges, *Renew. Sust. Energ. Rev.*, 2017, **69**, 771-789.

13. X. H. Zheng, Z. W. Zhu, X. Lin, Y. Zhang, Y. He, H. B. Cao and Z. Sun, A Mini-Review on Metal Recycling from Spent Lithium Ion Batteries, *Engineering*, 2018, **4**, 361-370.

14. R. N. Collins and A. S. Kinsela, The Aqueous Phase Speciation and Chemistry of Cobalt in Terrestrial Environments, *Chemosphere*, 2010, **79**, 763-771.

15. M. N. Hang, I. L. Gunsolus, H. Wayland, E. S. Melby, A. C. Mensch, K. R. Hurley, J. A. Pedersen, C. L. Haynes and R. J. Hamers, Impact of Nanoscale Lithium Nickel Manganese Cobalt Oxide (NMC) on the Bacterium Shewanella oneidensis MR-1, *Chem. Mat.*, 2016, **28**, 1092-1100.

16. J. Bozich, M. M. Hang, R. Hamers and R. Klaper, Core Chemistry Influences the Toxicity of Multicomponent Metal Oxide Nanomaterials, Lithium Nickel Manganese Cobalt Oxide, and Lithium Cobalt Oxide to *Daphnia magna*, *Environ. Toxicol. Chem.*, 2017, **36**, 2493-2502.

17. X. Huang, J. W. Bennett, M. M. N. Hang, E. D. Laudadio, R. J. Hamers and S. E. Mason, Ab Initio Atomistic Thermodynamics Study of the (001) Surface of LiCoO2 in a Water Environment and Implications for Reactivity under Ambient Conditions, *J. Phys. Chem. C*, 2017, **121**, 5069-5080.

18. Y. Cui, E. S. Melby, A. C. Mensch, E. D. Laudadio, M. M. N. Hang, A. Dohnalkova, D. H. Hu, R. J. Hamers and G. Orr, Quantitative Mapping of Oxidative Stress Response to Lithium Cobalt Oxide Nanoparticles in Single Cells Using Multiplexed in Situ Gene Expression Analysis, *Nano Lett.*, 2019, **19**, 1990-1997.

19. Z. V. Feng, B. R. Miller, T. G. Linn, T. Pho, K. N. L. Hoang, M. N. Hang, S. L. Mitchell, R. T. Hernandez, E. E. Carlson and R. J. Hamers, Biological impact of nanoscale lithium intercalating complex metal oxides to model bacterium B-subtilis, *Environ. Sci.-Nano*, 2019, **6**, 305-314.

20. E. V. Shkol'nikov, Thermodynamic characterization of the amphoteric oxides M2O3 (M = Cr, Fe, Co) and their hydrates in aqueous media, *Russian Journal of Applied Chemistry*, 2011, **84**, 1702-1709.

21. E. V. Shkol'nikov, Thermodynamic characterization of the amphoterism of oxides M2O3 (M = As, Sb, Bi) and Their hydrates in aqueous media, *Russian Journal of Applied Chemistry*, 2010, **83**, 2121-2127.

22. K. H. Gayer and A. B. Garrett, The Solubility of Cobalt Hydroxide, Co(OH)2, in Solutions of Hydrochloric Acid and Sodium Hydroxide at 25°, *Journal of the American Chemical Society*, 1950, **72**, 3921-3923.

23. S. Mitchell, N. Hudson-Smith, M. Cahill, B. Reynolds, S. Frand, C. Green, C. Y. Wang, M. N. Hang, R. T. Hernandez, R. J. Hamers, Z. V. Feng, C. Haynes and E. E. Carlson, Chronic exposure to complex metal oxide nanoparticles elicits rapid resistance in Shewanella oneidensis MR-1, *Chem. Sci.*, 2019, **10**, 9768-9781.

24. D. Sharan, D. Wolfson, C. M. Green, P. Lemke, A. G. Gavin, R. J. Hamers, Z. V. Feng and E. E. Carlson, Chronic exposure to complex metal oxide nanomaterials induces production of reactive oxygen species in bacteria, *Environ. Sci.-Nano*, 2023, **10**, 1978-1992.

25. J. I. Drever and L. L. Stillings, The Role of Organic Acids in Mineral Weathering, *Colloids and Surfaces A: Physiochemical and Engineering Aspects*, 1997, **120**, 167-181.

26. E. D. Flynn and J. G. Catalano, Reductive Transformations of Layered Manganese Oxides by Small Organic Acids and the Fate of Trace Metals, *Geochimica et Cosmochimica Acta*, 2019, **250**, 149-172.

27. G. J. Houben, Iron Oxide Incrustations in Wells. Part 2: Chemical Dissolution and Modeling, *Applied Geochemistry*, 2003, **18**, 941-954.

28. W. H. Huang and W. D. Keller, Dissolution of Rock-forming Silicate Minerals in Organic Acids: Simulated First-stage Weathering of Fresh Mineral Surfaces, *The American Mineralogist*, 1970, **55**, 2076-2094.

29. H. Dong, Mineral-microbe Interactions: A Review, *Frontiers of Earth Science in China*, 2010, **4**, 127-147.

30. Y. A. Gorby, F. Caccavo Jr. and H. Bolton Jr., Microbial Reduction of CobaltIIIEDTA- in the Presence and Absence of Manganese(IV) Oxide, *Environ Sci Technol*, 1998, **32**, 244-250.

31. J. E. Kostka and K. H. Nealson, Dissolution and Reduction of Magnetite by Bacteria, *Environ Sci Technol*, 1995, **29**, 2535-2540.

32. B. Ouyang, D. M. Akob, D. Dunlap and D. Renock, Microbially Mediated Barite Dissolution in Anoxic Brines, *Applied Geochemistry*, 2017, **76**, 51-59.

33.   E. Revesz, D. Fortin and D. Paktunc, Reductive Dissolution of Scorodite in the Presence of Shewanella sp. CN32 and Shewanella sp. ANA-3, *Applied Geochemistry*, 2015, **63**, 347-356.

34.   L. Shi, H. Dong, G. Reguera, H. Beyenal, A. Lu, J. Liu, H. Q. Yu and J. K. Fredrickson, Extracellular Electron Transfer Mechanisms between Microorganisms and Minerals, *Nat Rev Microbiol*, 2016, **14**, 651-662.

35.   S. L. Smith, B. M. Grail and D. B. Johnson, Reductive Bioprocessing of Cobalt-bearing Limonitic Laterites, *Minerals Engineering*, 2017, **106**, 86-90.

36.   M. Pourbaix, Atlas of Electrochemical Equilibria in Aqueous Solutions, *Journal of Electroanalytical Chemistry and Interfacial Electrochemistry*, 1967, **13**.

37.   E. D. Laudadio, P. Ilani-Kashkouli, C. M. Green, N. J. Kabengi and R. J. Hamers, Interaction of Phosphate with Lithium Cobalt Oxide Nanoparticles: A Combined Spectroscopic and Calorimetric Study, *Langmuir*, 2019, **35**, 16640-16649.

38.   S. Brunauer, P. H. Emmet and E. Teller, Adsorption of Gases in Multimolecular Layers, *Journal of the American Chemical Society*, 1938, **60**, 309-319.

39.   J. Bozich, M. Hang, R. Hamers and R. Klaper, Core chemistry influences the toxicity of multicomponent metal oxide nanomaterials, lithium nickel manganese cobalt oxide, and lithium cobalt oxide to *Daphnia magna*, *Environ. Toxicol. Chem.*, 2017, **36**, 2493-2502.

40.   E. D. Laudadio, J. W. Bennett, C. M. Green, S. E. Mason and R. J. Hamers, Impact of Phosphate Adsorption on Complex Cobalt Oxide Nanoparticle Dispersibility in Aqueous Media, *Environ Sci Technol*, 2018, **52**, 10186-10195.

41.   P. D. Reiss, P. F. Zuurendonk and R. L. Veech, Measurement of Tissue Purine, Pyrimidine, and Other Nucleotides by Radial Compression High-Performance Liquid Chromatography, *Analytical Biochemistry*, 1984, **140**, 162-171.

42.   K. Yamada, N. Hara, T. Shibata, H. Osago and M. Tsuchiya, The Simultaneous Measurement of Nicotinamide Adenine Dinucleotide and Related Compounds by Liquid Chromatography / Electrospray Ionization Tandem Mass Spectrometry, *Anal Biochem*, 2006, **352**, 282-285.

43.   A. H. Henke, E. D. Laudadio, J. K. Hedlund Orbeck, A. A. Tamijani, K. N. L. Hoang, S. E. Mason, C. J. Murphy, Z. V. Feng and R. J. Hamers, Reciprocal redox interactions of lithium cobalt oxide nanoparticles with nicotinamide adenine dinucleotide (NADH) and glutathione (GSH): toward a mechanistic understanding of nanoparticle-biological interactions, *Environmental Science: Nano*, 2021, **8**, 1749-1760.

44.   S. A. Löw, I. M. Löw, M. J. Weissenborn and B. Hauer, Enhanced Ene-Reductase Activity through Alteration of Artificial Nicotinamide Cofactor Substituents, *ChemCatChem*, 2016, **8**, 911-915.

45.   W. Xiao, R. S. Wang, D. E. Handy and J. Loscalzo, NAD(H) and NADP(H) Redox Couples and Cellular Energy Metabolism, *Antioxid Redox Signal*, 2018, **28**, 251-272.

46.   B. Chance, B. Schoener, R. Oshino, F. Itshak and Y. Nakase, Oxidation-Reduction Ratio Studies of Mitochondria in Freeze-trapped Samples, *Journal of Biological Chemistry*, 1979, **254**, 4764-4771.

47.   A. U. Rehman, A. G. Anwer, M. E. Gosnell, S. B. Mahbub, G. Liu and E. M. Goldys, Fluorescence Quenching of Free and Bound NADH in HeLa Cells Determined by Hyperspectral Imaging and Unmixing of Cell Autofluorescence, *Biomed Opt Express*, 2017, **8**, 1488-1498.

48.   D. A. Shirley, High-Resolution X-Ray Photoemission Spectrum of the Valence Bands of Gold, *Physical Review B*, 1972, **5**, 4709-4714.

49.   S. Tougaard, Practical guide to the use of backgrounds in quantitative XPS, *Journal of Vacuum Science & Technology A*, 2020, **39**, 011201.

50.   N. Fairley, V. Fernandez, M. Richard-Plouet, C. Guillot-Deudon, J. Walton, E. Smith, D. Flahaut, M. Greiner, M. Biesinger, S. Tougaard, D. Morgan and J. Baltrusaitis, Systematic and collaborative approach to problem solving using X-ray photoelectron spectroscopy, *Applied Surface Science Advances*, 2021, **5**, 100112.

51.   T. L. Barr and S. Seal, Nature of the use of adventitious carbon as a binding energy standard, *Journal of Vacuum Science & Technology A*, 1995, **13**, 1239-1246.

52.   R. F. Anderson, Energetics of the one-electron steps in the NAD+/NADH redox couple, *Biochimica et Biophysica Acta (BBA) - Bioenergetics*, 1980, **590**, 277-281.

53.   N. J. Kotloski and J. A. Gralnick, Flavin Electron Shuttles Dominate Extracellular Electron Transfer by Shewanella oneidensis, *mBio*, 2013, **4**, 4.

54.   H. von Canstein, J. Ogawa, S. Shimizu and J. R. Lloyd, Secretion of flavins by Shewanella species and their role in extracellular electron transfer, *Appl. Environ. Microbiol.*, 2008, **74**, 615-623.